Optical Society of America. Mark D. McNeill and Ting-Chung Poon, "Gaussian-beam profile shaping by acousto-optic Bragg diffraction," Appl. Opt. 33, 4508-4515 (1994). doi: 10.1364/AO.33.004508

Gaussian-beam profile shaping by acousto-optic Bragg diffraction

Mark D. McNeill and Ting-Chung Poon

We study how Gaussian laser-beam profiles can be modified into a desired form using acousto-optic Bragg diffraction. By exploiting the angular dependence of Bragg diffraction of plane waves by acoustic gratings, we demonstrate that the conversion from a Gaussian-profile beam into either a near-field or a far-field flattop profile is possible.

Introduction

Optical techniques used to convert the spatial intensity distribution of a Gaussian laser beam into a desirable flattop-type profile are important to many applications. These include laser fusion, laser printing, heat treatment of material surfaces, optical memory systems, laser radars with detector arrays, and optical data processing. Many methods have been proposed to generate flattop-type profiles either in the far-field or the near-field region.[1–12] Using the acousto-optic effect, Ohtsuka *et al.*[1,2] have been able to produce a uniform far-field distribution with the sound cell operating in the Raman–Nath regime.[13] Most recently, Tervonen *et al.* have improved the acousto-optic approach by utilizing the methods of synthetic diffractive optics.[12] In this paper we employ a multiple-plane-wave theory for strong acousto-optic interaction[13,14] together with a newly developed transfer-function formalism[15,16] to investigate how Gaussian intensity profiles can be transformed into either near-field or far-field flattop profiles by use of Bragg diffraction. Section 2 presents the multiple-plane-wave theory in terms of a set of infinite coupled differential equations and reviews the transfer-function formalism. Section 3 summarizes a general formalism for determining the output spatial profile from an arbitrary input field. Section 4 employs the transfer-function approach to explain the beam-distortion phenomen and shows that, under certain conditions, distortion can be eliminated by an increase in the strength of the sound field. Sections 5 and 6 identify the system parameters needed to convert the input Gaussian intensity profile into a flattop distribution in the near-field and far-field regions, respectively. Finally, Section 7 summarizes the findings and identifies the areas in which further research is needed.

The authors are with the Optical Image Processing Laboratory, Bradley Department of Electrical Engineering, Virginia Polytechnic Institute and State University, Blacksburg, Virginia 24061.

Received 8 July 1993; revised manuscript received 13 December 1993.

0003-6935/94/204508-08$06.00/0.

2. Korpel–Poon Multiple-Plane-Wave Scattering Theory and Transfer-Function Formalism

There are many possible theoretical approaches to the acousto-optic interaction problem. We have adopted the Korpel–Poon multiple-scattering theory[13,14] for the present investigation. The theory starts from the two-dimensional generalized Raman–Nath equations[13] and represents the light and sound fields as plane-wave decompositions together with a multiple scattering for the interaction. The general formalism is applicable not only to hologram-type configurations but also to physically realistic sound fields subject to diffraction. For a typical rectangular sound column with plane-wave incidence, as shown in Fig. 1, the general multiple-scattering theory can be reduced to the following infinite coupled equations:

$$\frac{d\tilde{E}_n}{d\xi} = -j\frac{\alpha}{2}\exp\left\{\frac{-j}{2}Q\xi\left[\frac{\phi_{inc}}{\phi_B} + (2n-1)\right]\right\}\tilde{E}_{n-1} - j\frac{\alpha}{2}\exp\left\{\frac{j}{2}Q\xi\left[\frac{\phi_{inc}}{\phi_B} + (2n+1)\right]\right\}\tilde{E}_{n+1}, \quad (1)$$

with the boundary condition $\tilde{E}_n = \tilde{E}_{inc}\delta_{n0}$ at $z \le 0$, where δ_{n0} is the Kronecker delta and $\tilde{E}_n$ is the complex amplitude of the nth-order plane wave of light in the direction $\phi_n = \phi_{inc} + 2n\phi_B$. ϕ_{inc} is the incident angle of the plane wave, $\tilde{E}_{inc}$, and ϕ_B is the Bragg angle,

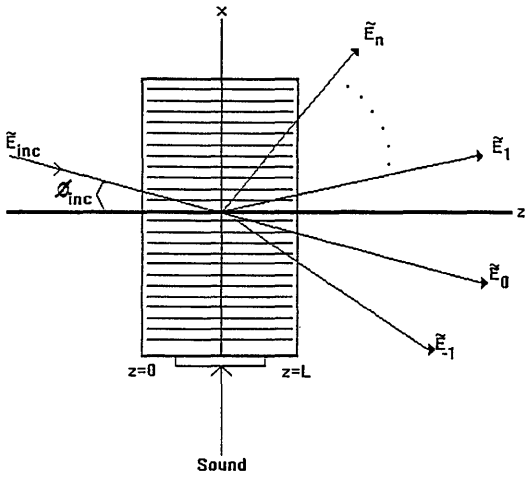

Fig. 1. Sound–light interaction configuration.

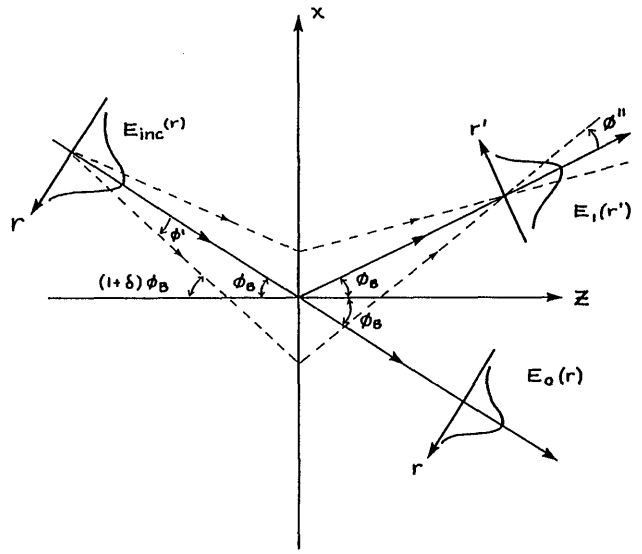

Fig. 2. Diffraction geometry for upshifted Bragg operation.

defined as $\phi_B = \lambda/2\Lambda$, where λ and Λ denote the wavelenghts of light and sound inside the acoustic medium, respectively. The other parameters in Eq. (1) are defined as follows: $\alpha = CkSL/2$ is the peak phase delay through the medium, where C represents the strain-optic coefficient of the medium, k is the propagation constant of the light in the medium, S is the amplitude of the sound field, and L is the width of the sound column. $Q = 2\pi L\lambda/\Lambda^2$ is the Klein Cook parameter.[17] Lastly, $\xi = L/z$ is the normalized distance inside the sound cell. $\xi = 0$ signifies when a plane wave of light enters into the acousto-optic cell, and $\xi = 1$ denotes when a plane wave of light exists from the cell.

Equation (1) is similar to the well-known Raman–Nath equations.[18] In fact, it can be shown[13] to be identical to the approximate [i.e., retaining no terms higher than $(\lambda/\Lambda)^2$] Raman–Nath equations. It is physically obvious that Eq. (1) identifies the plane-wave contributions to $\tilde{E}_n$ from neighboring orders, with the phase terms indicating the degree of phase mismatch. It is a special case of the general multiple-scattering theory[13,14] valid for any sound field, not just a sound column. Note that Eq. (1) is valid only for small diffraction angles (i.e., paraxial approximation). For a given value of α and Q the solution to Eq. (1) represents the contributions to the nth-order plane wave of light, $\tilde{E}_n$, owing to the plane wave $\tilde{E}_{inc}$ incident at ϕ_{inc}. Note that the sign convention for ϕ_{inc} is counterclockwise positive; that is $\phi_{inc} = -\phi_B$ signifies upshifted Bragg diffraction.

Choosing $\phi_{inc} = -(1 + \delta)\phi_B$, where δ represents the deviation of the incident plane wave away from the Bragg angle, as illustrated in Fig. 2, and limiting ourselves to $\tilde{E}_0$ and $\tilde{E}_1$, we have the following set of coupled differential equations:

$$\frac{d\tilde{E}_0}{d\xi} = -j\frac{\alpha}{2}\exp(-jQ\xi\delta/2)\tilde{E}_1, \tag{2a}$$

$$\frac{d\tilde{E}_1}{d\xi} = -j\frac{\alpha}{2}\exp(jQ\xi\delta/2)\tilde{E}_0. \tag{2b}$$

Equations (2a) and (2b) can be solved analytically, and the solutions are given by the well-known Phariseau formula[19]:

$$\tilde{E}_0(\xi) = \tilde{E}_{inc}\exp(-j\delta Q\xi/4)\left\{\cos[(\delta Q/4)^2 + (\alpha/2)^2]^{1/2}\xi + j\frac{\delta Q}{4}\frac{\sin[(\delta Q/4)^2 + (\alpha/2)^2]^{1/2}\xi}{[(\delta Q/4)^2 + (\alpha/2)^2]^{1/2}}\right\}, \tag{3a}$$

$$\tilde{E}_1(\xi) = \tilde{E}_{inc}\exp(j\delta Q\xi/4) \times\left\{-j\frac{\alpha}{2}\frac{\sin[(\delta Q/4)^2 + (\alpha/2)^2]^{1/2}\xi}{[(\delta Q/4)^2 + (\alpha/2)^2]^{1/2}}\right\}. \tag{3b}$$

Equations (3a) and (3b) are similar to the standard two-wave solutions found by Aggarwal[20] and adapted by Kogelnik[21] to holography. More recently, it has been rederived with the Feynman diagram technique.[14] Equations (3a) and (3b) represent the plane-wave solutions that are due to oblique incidence, and by letting $\delta = 0$ we can reduce them to the following set of well-known expressions for ideal Bragg diffraction:

$$\tilde{E}_0 = \tilde{E}_{inc}\cos\left(\frac{\alpha}{2}\xi\right), \tag{4a}$$

$$\tilde{E}_1 = -j\tilde{E}_{inc}\sin\left(\frac{\alpha}{2}\xi\right). \tag{4b}$$

Equation (3) motivated Poon and Chatterjee[15,16] to define the so-called plane-wave transfer function of the Bragg cell on which a light beam with an arbitrary profile is incident. The transfer functions of the zeroth-order and the first-order light are defined,

respectively, as follows:

$$H_0(\delta) = \frac{\tilde{E}_0(\xi)|_{\xi=1}}{\tilde{E}_{\text{inc}}}, \tag{5a}$$

$$H_1(\delta) = \frac{\tilde{E}_1(\xi)|_{\xi=1}}{\tilde{E}_{\text{inc}}}, \tag{5b}$$

where $\tilde{E}_0(\xi)$ and $\tilde{E}_1(\xi)$ are, in general, the results from Eq. (1) evaluated at the exit of the Bragg cell. For relatively low sound pressures, analytical results from Eqs. (3a) and (3b) can be used to expedite computer calculations. This definition of the transfer function permits us to relate the input angular spectrum, $\tilde{E}_{\text{in}}(\delta)$, to the output spectrum, $\tilde{E}_{\text{out}}(\delta)$, as

$$\tilde{E}_{\text{out}}(\delta) = \tilde{E}_{\text{in}}(\delta)H(\delta). \tag{6}$$

For a specific diffracted order of light we need only replace $H(\delta)$ in Eq. (6) by the appropriate transfer function, for example, $H_0(\delta)$ or $H_1(\delta)$, and then permit $\tilde{E}_{\text{out}}(\delta)$ to become $\tilde{E}_0(\delta)$ or $\tilde{E}_1(\delta)$, respectively. Note that this transfer-function approach has recently been extended to include the propagational diffraction effect[22] and the case of large Bragg angles.[23]

3. General Formalism for Arbitrary Incident Light Fields

This section serves to summarize the techniques[15,16] used to calculate the spatial profile of any diffracted order using strong acousto-optic interaction. To find the input angular spectrum, we refer to the coordinate system introduced in Fig. 2, which illustrates how an arbitrary incident field propagates through a Bragg cell operating in the upshifted mode. The incident field is decomposed into multiple plane waves with different amplitudes propagating in directions defined by $\phi' = \delta\phi_B$. We relate the angular spectrum $\tilde{E}(\phi')$, under paraxial approximation, to the spatial distribution $E(r)$ as follows:

$$E(r) = F^{-1}[\tilde{E}(\phi')] = \int_{-\infty}^{\infty} \tilde{E}(\phi')\exp\left(-j\frac{2\pi}{\lambda}\phi' r\right)\mathrm{d}\left(\frac{\phi'}{\lambda}\right), \tag{7a}$$

$$\tilde{E}(\phi') = F[E(r)] = \int_{-\infty}^{\infty} E(r)\exp\left(j\frac{2\pi}{\lambda}\phi' r\right)\mathrm{d}r, \tag{7b}$$

where $(r, \phi'/\lambda)$ represent the transform variables.

Equations (6)–(7b) may be combined to develop a general formalism for computing the profiles of any scattered light field in the spatial domain from any arbitrary input field. For the zeroth-order light,

$$E_0(r) = \int_{-\infty}^{\infty} \tilde{E}_{\text{in}}(\delta)H_0(\delta)\exp\left(-j2\pi\frac{\delta}{2\Lambda}r\right)\mathrm{d}\left(\frac{\delta}{2\Lambda}\right), \tag{8a}$$

and for the first-order light,

$$E_1(r') = \int_{-\infty}^{\infty} \tilde{E}_{\text{in}}(\delta)H_1(\delta)\exp\left(j2\pi\frac{\delta}{2\Lambda}r'\right)\mathrm{d}\left(\frac{\delta}{2\Lambda}\right), \tag{8b}$$

where we substitute $\delta\phi_B$ for ϕ' in the case of the zeroth-order light and $-\delta\phi_B$ for ϕ'' in the case of the first-order light when Eqs. (7a) and (7b) are used. This is consistent with the diffraction geometry defined in Fig. 2. In writing the final form of Eqs. (8a) and (8b) we also used $\lambda/2\Lambda$ for ϕ_B. It is important to note that we chose $H_0(\delta)$ and $H_1(\delta)$ as special cases. For any diffracted order we may find $H_n(\delta)$ first by solving Eq. (1) for that particular value of n, using the definition of Eqs. (5a) and (5b), and then by substituting that solution into Eqs. (8a) and (8b). Hence, Eqs. (1), (8a), and (8b) form a complete set of analytical tools for determining the profile of any output scattered field from any arbitrary input field in the presence of a strong acoustic field. This technique is reminiscent of the Fourier decomposition method developed independently by Magdich and Molchanov.[24] The technique has been reviewed by Benlarbi *et al.*,[25] in their study only two scattered beams are considered and hence may not be accurate for high values of the sound field. Returning to the beam-shaping problem, we see in Eqs. (8a) and (8b) that the transfer function can modify the output profile by variation of α and Q. Indeed, by properly choosing α and Q, we shall demonstrate that an input Gaussian-beam profile can be converted into a desirable flattop-type profile. Because this formalism involves the Fourier transform, a fast-Fourier-transform algorithm is used to calculate the output field distribution corresponding to a variety of arbitrary incident field profiles.

4. Transfer Functions and Beam Distortion

In this section we investigate the behavior of $H_1(\delta)$, and on the basis of these results we explain the beam-distortion phenomena.[15,16,26–32] Equation (1) provides the starting point for our general theory. Although Eq. (1) involves a set of infinite coupled differential equations, the effect of including more than two diffracted orders is diminished significantly as the value of Q increases. For example, we calculated the transfer functions and compared the solutions for ten orders (i.e., $-4 \le n \le 5$) to well-known ideal solutions for two orders [see Eqs. (3a) and (3b)] and found that when $Q > 40$, the solutions were nearly identical in $|\delta| \le 0.5$ for α values of up to 4π. For $Q = 20$, Figs. 3(a) and 3(b) show the magnitude of $H_1(\delta)$ produced by solving Eq. (1) with two orders and ten orders, respectively. We employed a fifth-order Runge–Kutta numerical method to find the solution to Eq. (1). Note that the two plots have nearly the same shape along the δ axis for small values of α. For large values of α the plot with a higher number of diffracted orders tend to expand more along the α axis as well as distort some features along δ. This suggests that higher diffracted orders are necessary to

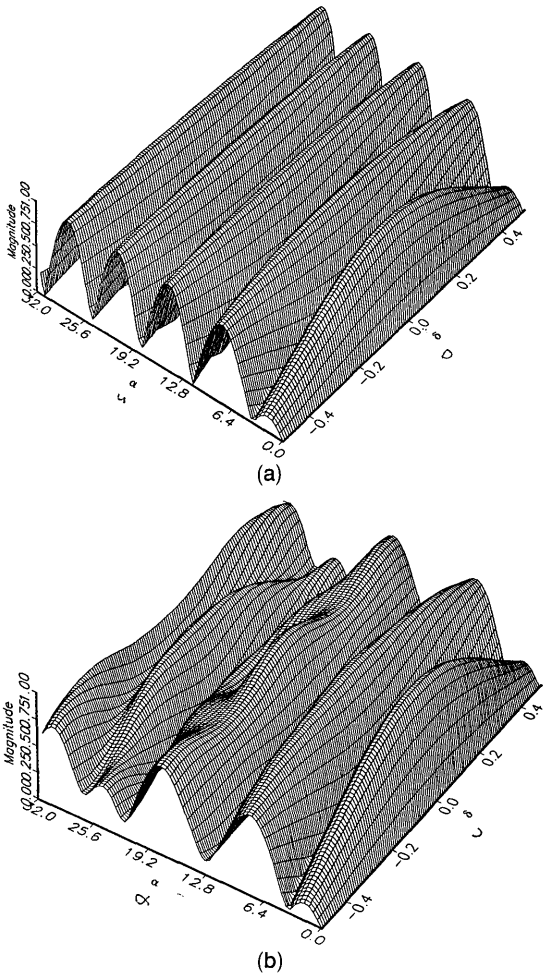

Fig. 3. Numerical plots of $|H_1(\delta)|$ as a function of the peak phase delay, α, for $Q = 20$: (a) solution involving two diffracted orders, (b) solution involving ten diffracted orders.

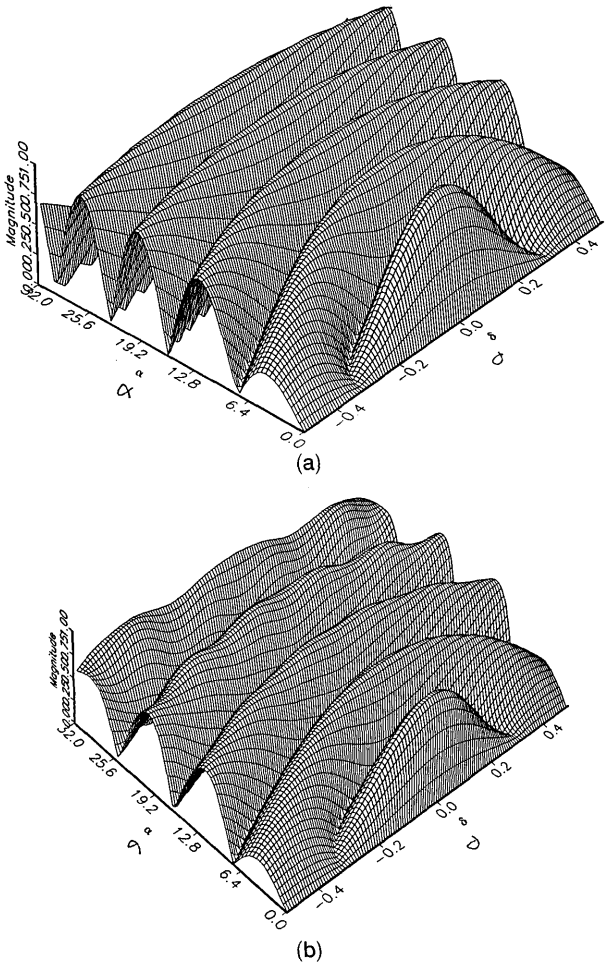

Fig. 4. Numerical plots of $|H_1(\delta)|$ as a function of α for $Q = 40$: (a) solution involving two diffracted orders, (b) solution involving ten diffracted orders.

calculate the appropriate transfer functions for applications involving large values of α. Similar behaviors are observed for $Q = 40$, as shown in Fig. 4. Results indicate that when $Q > 40$ for the range of α investigated, solutions involving two and ten diffracted orders are indiscernible. Hence, when computing the magnitude of $H_1(\delta)$ for $Q > 40$ at small values of α, we solved Eq. (1) numerically while limiting it to only two orders to accelerate the computer calculations.

Figure 5 shows how larger value of Q modify the spectrum of the transfer function. Notice how the zeros of the transfer function move inward as the value of Q is increased. The location of these zeros, particularly the first zeros, determines how severely the system distorts the profile of the input field. As an example, we inspect one of the plots for a large value of Q, say Fig. 5(b), for the case when $Q = 160$. Because of the Fourier-transform relationship, a narrower beam in the spatial domain leads to a wider spread in the angular spectrum domain. If this spread is large enough to cover some of the zeros in $H_1(\delta)$, distortion in the spatial domain of the Bragg-scattered light profile is expected. Specifically, let us assume that the incident Gaussian light field $E_{in}(r)$ is given by

$$E_{in}(r) = \frac{E_{inc}}{\sigma_1(2\pi)^{1/2}} \exp(-r^2/2\sigma_1{}^2), \tag{9}$$

where r is the radial coordinate shown in Fig. 2. Its angular spectrum, according to Eq. (7b) with $\phi' = \delta\phi_B = \delta\lambda/2\Lambda$, becomes

$$\tilde{E}_{in}(\delta) = E_{inc} \exp\left[-\frac{1}{2}\left(\frac{\pi\sigma_1}{\Lambda}\right)^2 \delta^2\right]. \tag{10}$$

For $\sigma_1/\Lambda = 5$ the $1/e$ point of the angular spectrum is given by $\delta_{1/e} = \sqrt{2}\Lambda/\pi\sigma_1 \approx 0.09$. Now, when operating with Bragg cells, one would like to work with maximum diffraction into the first order. This point of operation occurs when the value of α is an odd multiple of π for cells with a large Q value. Looking at Fig. 5(b), we can see that the angular spread of the incident beam spans beyond the first zero of $|H_1(\delta)|$ for $\alpha = \pi$. Physically, it means that some plane

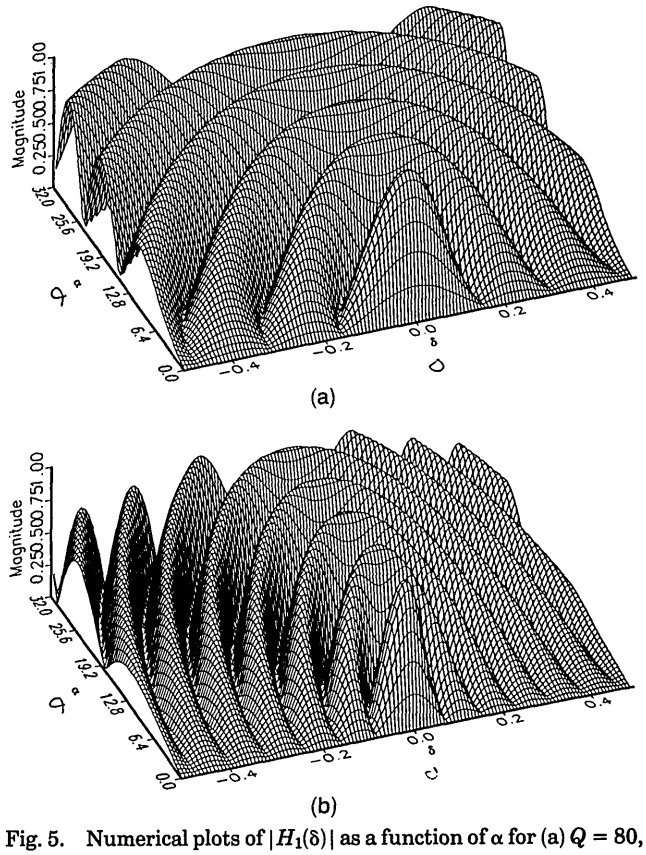

Fig. 5. Numerical plots of $|H_1(\delta)|$ as a function of α for (a) $Q = 80$, (b) $Q = 160$.

waves of the beam are not scattered at all. Therefore reconstruction of the beam at the exit of the Bragg cell may show distortion. To avoid this distortion, one may work with $\alpha = 3\pi$ instead of $\alpha = \pi$ because the transfer function in Fig. 5(b) indicates that the first zero of the transfer function has moved beyond $\delta_{1/e}$ at $\alpha = 3\pi$. Before verifying this point, it is instructive to develop an explicit expression that represents the diffracted field. This is done by substitution of Eq. (10) into Eq. (8b) and the use of Eq. (5b) to obtain the following expression for $E_1(r')$:

$$E_1(r') = \int_{-\infty}^{\infty} E_{\text{inc}} \exp\left[-\frac{1}{2}\left(\frac{\pi\sigma_1}{\lambda}\right)^2 \delta^2\right] \left\{\left(-j\frac{\alpha}{2}\right)\exp(j\delta Q/4) \times \text{sinc}[(\delta Q/4)^2 + (\alpha/2)^2]^{1/2}\right\} \times \exp\left(j2\pi\frac{\delta}{2\Lambda}r'\right) d\left(\frac{\delta}{2\Lambda}\right), \quad (11)$$

where $(-r', \delta/2\Lambda)$ may be identified as the Fourier-transform variables. Figure 6 plots the normalized intensity profile of the Bragg-scattered beam, $I_1(r') = |E_1(r')|^2$. The input Gaussian has also been plotted at the center of the two output beams as a reference. Notice that the output profile is distorted more at $\alpha = \pi$ than it is at $\alpha = 3\pi$. That is, the profile still has somewhat of a Gaussian shape at $\alpha = 3\pi$; in fact, it has a low-pass version of the input Gaussian beam.

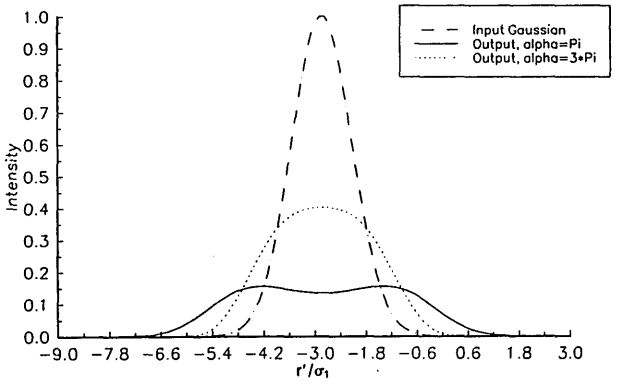

Fig. 6. Beam distortion of input Gaussian beam profile and its disappearance: Distortion occurs at $\alpha = \pi$ but disappears at the stronger sound pressure, $\alpha = 3\pi$. $\sigma_1/\Lambda = 4.5$, $Q = 160$.

The discussion above illustrates beam distortion in the Bragg-scattered beam when either a thick hologram or an acousto-optic Bragg cell is illuminated by a narrow laser beam.[26,32] Thus, by inspecting the transfer function for a specific Q of the Bragg cell and the size of the incident beam σ_1, one can predict this distortion phenomena intuitively without recourse to complicated mathematics.

5. Flattop Profile Shaping in the Near Field

This section deals with the selection of Q, α, and σ_1/Λ necessary to achieve a flattop beam profile in the near field for the Bragg-scattered beam when the incident beam is assumed to be Gaussian. To achieve this desired shape, Eq. (6) should become approximately a sinc(δ)-type distribution; that is, we want

$$F^{-1}[\tilde{E}_{\text{in}}(\delta)H_{\text{req}}(\delta)] = \text{rect}\left(\frac{r}{\sigma_0}\right), \quad (12)$$

where σ_0 denotes the width of the output flattop beam. Taking the Fourier transform of both sides leads to the required transfer function, $H_{\text{req}}(\delta)$. This equation along with $H_1(\delta)$ represents the design equations

$$H_{\text{req}}(\delta) = \text{sinc}\left(\sigma_0\frac{\delta}{2\Lambda}\right)\left\{\exp\left[\frac{1}{2}\left(\pi\frac{\sigma_1}{\Lambda}\delta\right)^2\right]\right\}, \quad (13a)$$

$$H_1(\delta) = \text{sinc}[(\delta Q/4)^2 + (\alpha/2)^2]^{1/2}, \quad (13b)$$

where $\text{sinc}(x) = \sin(x)/x$. Note that in writing Eq. (13b), we neglect the constant and the phase factor in front of the sinc function [see Eqs. (3b) and (5b)]. The phase factor in Eq. 3(b) merely introduces a spatial shift of the diffracted beam, as is evident from the results in Fig. 6, in which the center of the scattered beam is shifted to the negative region of r' (see Fig. 2). In design problems one would like to find $H_1(\delta)$ such that it matches $H_{\text{req}}(\delta)$ as best as possible. By inspecting the general behavior of $H_1(\delta)$ and $H_{\text{req}}(\delta)$ as a function of α for a specific value of Q, one can choose the tuning parameters such that these expressions are approximately equal. A criterion

that seems to work well is to choose the first zeros of Eqs. (13a) and (13b) to coincide with the $1/e$ point of the input Gaussian spectrum, $\delta_{1/e}$. This permits enough energy into the sidelobes of the sinc function for $H_1(\delta)$ to achieve a flattop distribution. The $1/e$ point of the input Gaussian spectrum and the first zeros of $H_{\text{req}}(\delta)$ and $H_1(\delta)$, respectively, are

$$\delta_{1/e} = \frac{\sqrt{2}\Lambda}{\pi\sigma_1}, \tag{14a}$$

$$\delta_{\text{req}} = \frac{2\Lambda}{\sigma_0}, \tag{14b}$$

$$\delta_1 = \frac{4}{Q}[(n\pi)^2 - (\alpha/2)^2]^{1/2}. \tag{14c}$$

Note, n is an integer in Eq. (14c). It reflects the fact that when α is sufficiently large, the first zero of $H_1(\delta)$ in Eq. (13b) becomes a multiple of π. This is evident from Fig. 5. Because $\delta_{1/e}$ is known for a given input beam, Q and α, according to Eqs. (14b) and (14c), assume the following expressions:

$$Q = \frac{4\pi}{\sqrt{2}}\frac{\sigma_1}{\Lambda}[(n\pi)^2 - (\alpha/2)^2]^{1/2}, \tag{15a}$$

$$\alpha = 4\left[(n\pi)^2 - \frac{1}{8}\left(\frac{Q\Lambda}{\pi\sigma_1}\right)^2\right]^{1/2}. \tag{15b}$$

Since $\delta_{\text{req}} = \delta_{1/e}$ is required in the criterion, this stipulates that the output flattop beam profile has an effective width $\sigma_0 = (2/\sqrt{2})\pi\sigma_1$. Figure 7 shows the effect of using the criterion for $\alpha = \pi$ and $(\sigma_1/\Lambda) = 10$. Although it is ideal for $\tilde{E}_{\text{in}}(\delta)H_1(\delta)$ to resemble a sinc(x)-type distribution, it is shown here that the Gaussian curve actually suppresses the sidelobes of $H_1(\delta)$. Figure 8(a) shows a flattop Bragg-scattered beam profile. The value of Q is calculated to be 242. Figure 8(b) shows that as the input Gaussian becomes narrower (i.e., σ_1/Λ is reduced to 4), the value of Q needed to make a flattop decreases to 97. This flatness of the output profile can be improved by a change in α with the sound pressure or of Q with the sound frequency. Figure 9 shows the effect of fine tuning α or Q to achieve a better flattop but with a sacrifice in the beam intensity.

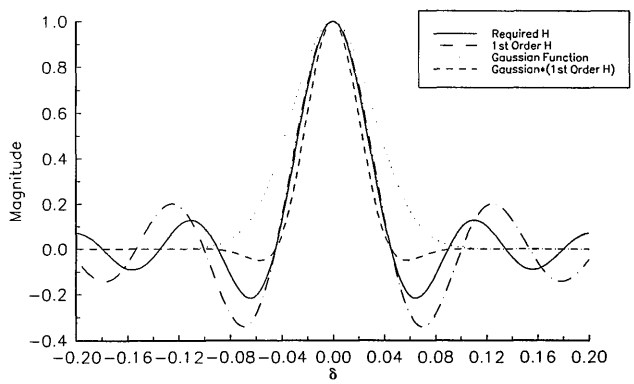

Fig. 7. Design curves showing the $1/e$ point of the input Gaussian spectrum coincide with the first zeros of $H_{\text{req}}(\delta)$ and $H_1(\delta)$. Q = 242, $\sigma_1/\Lambda = 10$, $\alpha = \pi$.

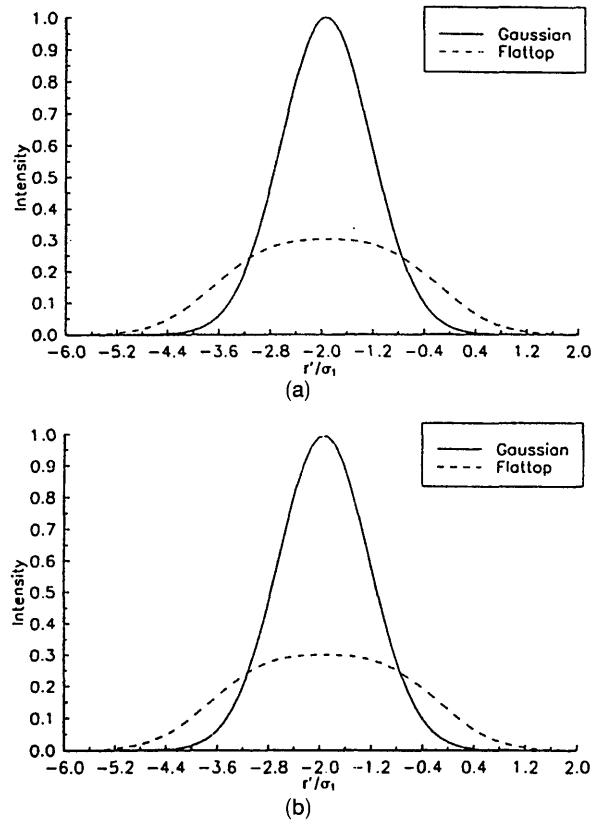

Fig. 8. Near-field flattop for (a) $\sigma_1/\Lambda = 10$, $Q = 242$, and (b) $\sigma_1/\Lambda = 4$, $Q = 97$, illustrating that a thinner Gaussian input beam requires a smaller Q value to achieve a flattop output. In both (a) and (b), $\alpha = \pi$.

6. Flattop Beam Profile in the Far Field

In order to achieve a flattop profile in the far field, one must approximate $\tilde{E}_{\text{in}}(\delta)H_{\text{req}}(\delta)$ by a rectangular function at the exist of the Bragg cell. That is, if we can find a flattop in the δ domain, it will appear as a flattop spatial profile in the far field. The relation-

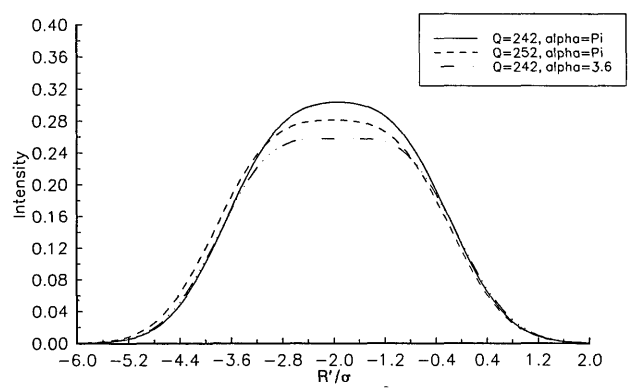

Fig. 9. More uniform flattop outputs obtained by the fine tuning of Q or α for the case shown in Fig. 8(a).

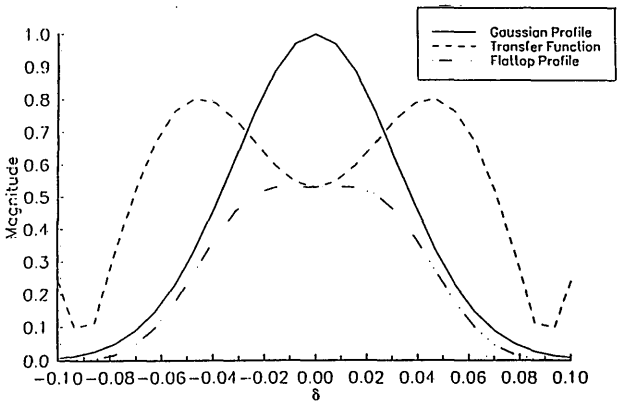

Fig. 10. Far-field flattop generation for an output beam profile obtained by a depression in the transfer function to offset the Gaussian peak. $\sigma_1/\Lambda = 10$, $Q = 225$, $\alpha = 7.4$.

ship that must be achieved is given by the following equation:

$$\tilde{E}_{\text{in}}(\delta)H_{\text{req}}(\delta) = \text{rect}\left(\frac{\delta}{\sigma_0}\right). \tag{16}$$

Therefore one must find $H_{\text{req}}(\delta)$ by inspecting $H_1(\delta)$ so that Eq. (16) is approximately satisfied. Because the Gaussian wave has a maximum at the center, there is a need to find a point in $H_1(\delta)$ at which a depression occurs such that it nullifies this amplitude increase. Although it is difficult to find an expression to predict this event, it is possible to view plots of $H_1(\delta)$ for different values of Q in order to select a curve that may approximately satisfy Eq. (16). For example, by inspection of the transfer function when $Q = 160$ [see Fig. 5(b)], it is apparent that a u-shaped distribution forms when α is between 2π and 3π. Thus we may search for a value of α within these limits to find the correct u shape to offset the Gaussian peak. Figure 10 shows the results of this approach at $Q = 225$ and $\alpha = 7.4$; the output angular spectrum has a flattop distribution at the exit of the Bragg cell.

7. Conclusion

Using a multiple-plane-wave scattering formalism for operation in the Bragg regime, we have developed a general technique to predict the spatial profile of a diffracted beam. This technique is based on the Fourier-transform theory and the plane-wave transfer function. For the specific case of a Gaussian incident light beam, simulation results show that a flattop profile could be produced by variation of either the pressure (α) or the frequency (Q) of the sound signal. The theory presented shows that it is possible to design systems by use of acousto-optic Bragg cells to satisfy both the near-field and the far-field requirements. Further research in this area shall involve experimental results to verify the approach. Also, there is a need to extend applications beyond those converting Gaussian input profiles to flattop profiles. That is, more attention should be concentrated on how arbitrary input profiles can be shaped into any desired output profiles, not limited to flattops. This has immediate applications in developing programmable spatial light modulators for image processing and pattern recognition. The transfer-function approach presented here serves to provide an intuitive insight into the problem.

A NASA graduate fellowship (Marshall Space Flight Center, Alabama) awarded to M. McNeill is appreciated.

References

1. Y. Ohtsuka and A. Tanone, "Acousto-optic intensity modification of a Gaussian laser beam," Opt. Commun. **39,** 70–74 (1981).
2. Y. Ohtsuka, A. Yasatomo, and Y. Imai, "Acousto-optic two-dimensional profile shaping of a Gaussian laser beam," Appl. Opt. **24,** 2813–2819 (1985).
3. C.-Y. Han, Y. Ishii, and K. Murata, "Reshaping collimated laser beams with Gaussian profile to uniform profiles," Appl. Opt. **22,** 3644–3647 (1983).
4. W. B. Veldkamp and C. J. Kastner, "Beam profile shaping for laser radars that use detector arrays," Appl. Opt. **21,** 345–355 (1982).
5. W. B. Veldkamp, "Laser beam profile shaping with interlaced diffraction gratings, "Appl. Opt. **21,** 3209–3212 (1982).
6. D. Shafer, "Gaussian to flattop intensity distributing lens," Opt. Laser Technol. **14,** 159–160 (1982).
7. L. E. Hargrove, "Effects of ultrasonic waves on Gaussian light beams with diameter comparable to ultrasonic wavelength," J. Acoust. Soc. Am. **43,** 847–851 (1967).
8. S. R. Jahan and M. A. Karim, "Refracting systems for Gaussian-to-uniform beam transformations," Opt. Laser Technol. **21,** 27–30 (1989).
9. M. A. Karim, A. M. Hanafi, F. Hussain, S. Mustafa, Z. Samberid, and N. M. Zain, "Realization of a uniform circular source using a two-dimensional binary filter," Opt. Lett. **10,** 470–472 (1985).
10. B. R. Frieden, "Lossless conversion of a plane laser wave to a plane wave of uniform irradiance," Appl. Opt. **4,** 1400–1403 (1965).
11. R. L. Aagard, "Methods of optimizing the beam shape in a focused coherent optical system," Appl. Opt. **13,** 1633–1638 (1974).
12. E. Tervonen, A. T. Friberg, and J. Turunen, "Acousto-optic conversion of laser beams into flat-top beams," J. Mod. Opt. **40,** 625–635 (1993).
13. A. Korpel, *Acousto-Optics* (Dekker, New York, 1988), pp. 95–121.
14. T.-C. Poon and A. Korpel, "Feynman diagram approach to acousto-optic scattering in the near-Bragg region," J. Opt. Soc. Am. **71,** 1202–1208 (1981).
15. T.-C. Poon and M. R. Chatterjee, "Transfer function approach to acousto-optic Bragg diffraction of finite optical beams using Fourier integrals," presented at the 1988 International Union of Radio Science Meeting, Syracuse, N.Y., June 1988.
16. M. R. Chatterjee, T.-C. Poon, and D. N. Sitter, "Transfer function formalism for strong acousto-optic Bragg diffraction of light beams with arbitrary profiles," Acustica **71,** 81–92 (1990).
17. W. R. Klein and B. D. Cook, "Unified approach to ultrasonic light diffraction," IEEE Trans. Sonics Ultrason. **SU-14,** 723–733 (1967).
18. C. V. Raman and N. S. N. Nath, "The diffraction of light by high frequency sound waves," Proc. Indian Acad. Sci. Sect. A **2,** 406–420 (1935); **3,** 75–84, 119–125, 459–465 (1936).
19. P. Phariseau, "On the diffraction of light by progressive

supersonic waves," Proc. Indian Acad. Sci. Sect. A **44,** 165–170 (1956).
20. R. R. Aggarwal, "Diffraction of light by ultrasonic waves (deduction of different theories from the generalized theory of Raman and Nath)," Proc. Indian Acad. Sci. Sect. A **31,** 417–426 (1950).
21. H. Kogelnik, "Coupled wave theory for thick hologram gratings," Bell Syst. Tech. J **48,** 2909–2947 (1969).
22. P. P. Banerjee and C. Tarn, "A Fourier transform approach to acousto-optic interaction in the presence of propagational diffraction," Acustica **74** 181–191 (1991).
23. S. Min and M. R. Chatterjee, "General integral formalism for acousto-optic and holographic Bragg scattering for arbitrary profiles and orientations," Acustica **71,** 81–92 (1990).
24. L. N. Magdich and V. Y. Molchanov, "Diffraction of a divergent beam by intense acoustic waves," Opt. Spectrosc. (USSR) **42,** 299–302 (1977).
25. B. Benlarbi, P. St. J. Russell, and L. Solymar, "Bragg diffraction of finite beams by thick gratings: two rival theories," Appl. Phys. B **28,** 63–72 (1982).
26. M. R. Forshaw, "Diffraction of a narrower laser beam by a thick hologram: experimental results," Opt. Commun. **12,** 279–281 (1974).
27. R. S. Chu and T. Tamir, "Bragg diffraction of Gaussian beams by periodically modulated media," J. Opt. Soc. Am. **66,** 220–226 (1976).
28. R. S. Chu and T. Tamir, "Bragg diffraction of Gaussian beams by periodically modulated media for incidence close to a Bragg angle," J. Opt. Soc. Am. **66,** 1438–1440 (1976).
29. R. S. Chu, J. A. Kong, and T. Tamir, "Diffraction of Gaussian beams by a periodically modulated layer," J. Opt. Soc. Am. **67,** 1555–1561 (1977).
30. M. G. Moharam, T. K. Gaylord, and R. Magnusson, "Bragg diffraction of finite beams by thick gratings," J. Opt. Soc. Am. **70,** 300–304 (1980).
31. B. Benlarbi, P. St. J. Russell, and L. Solymar, "Bragg diffraction of Gaussian beams by thick gratings: numerical evaluations by plane-wave decomposition," Appl. Phys. B **28,** 383–390 (1982).
32. D. G. Hawkins, "Finite beamwidth effects in bulk acousto-optic interactions," J. Opt. Soc. Am. A **70,** 1611 (1980).